J|A|C|S
ARTICLES
Published on Web 08/03/2002

Structure of $V_2O_5 \cdot nH_2O$ Xerogel Solved by the Atomic Pair Distribution Function Technique

Valeri Petkov,[†] Pantelis N. Trikalitis,[§] Emil S. Bozin,[†] Simon J. L. Billinge,[†] Thomas Vogt,[‡] and Mercouri G. Kanatzidis*[,§]

Contribution from the Department of Physics and Astronomy and Center for Fundamental Materials Research, Michigan State University, East Lansing, Michigan 48824, Physics Department, Brookhaven National Laboratory, Upton, New York 11973, and Department of Chemistry and Center for Fundamental Materials Research, Michigan State University, East Lansing, Michigan 48824

Received March 8, 2002

Abstract: A long-standing issue regarding the local and long-range structure of $V_2O_5 \cdot nH_2O$ xerogel has been successfully addressed. The full three-dimensional structure of the lamellar turbostratic $V_2O_5 \cdot nH_2O$ xerogel was determined by the atomic pair distribution function technique. We show that on the atomic scale the slabs of the xerogel can be described well as almost perfect pairs (i.e., bilayers) of single V_2O_5 layers made of square pyramidal VO_5 units. These slabs are separated by water molecules and stack along the *z*-axis of a monoclinic unit cell (space group *C*2/*m*) with parameters $a = 11.722(3)$ Å, $b = 3.570(3)$ Å, $c = 11.520(3)$ Å, and $\beta = 88.65°$. The stacking sequence shows signatures of turbostratic disorder and a structural coherence limited to 50 Å.

Introduction

The versatile redox, intercalation, swelling, and electrical properties of $V_2O_5 \cdot nH_2O$ xerogel have fascinated researchers for many decades[1] and inspired an intensive search for potential applications such as chemical sensors,[2] electrochemical and fast switching devices,[2,3] and reversible high-energy density lithium ion batteries.[4] The xerogel has been used as a host material for a large variety of atomic and molecular species and even electronically conducting and insulating polymers.[5] Despite decades of experimentation with $V_2O_5 \cdot nH_2O$, its atomic structure has remained somewhat of a mystery because it does not form crystals and exists only as ribbonlike particles about 10 nm wide and 1 μm long,[1] Figure 1a. Nevertheless, the xerogel is not amorphous and displays lamellar ordering (albeit turbostratic) as indicated by the pronounced 00*l* reflections observed in a typical XRD pattern of the xerogel, Figure 1b. The limited diffraction pattern, with no sharp Bragg peaks, makes it impossible to determine the three-dimensional (3-D) atomic structure by traditional crystallographic techniques. However, the pattern contains a small number of Bragg-like features, indicating the presence of intermediate range order and a pronounced diffused component, Figure 2a. These are characteristics of "nanocrystalline" materials that have well-ordered local structures, but the structural coherence is limited to the nanometer length scale.[6] The structure of the $V_2O_5 \cdot nH_2O$ xerogel is an important scientific issue because its elucidation is a key prerequisite to a better understanding and exploitation of its properties.

Despite these difficulties, two competing structural models have been put forward for $V_2O_5 \cdot nH_2O$. Livage et al. proposed that the xerogel, on the atomic scale, is a stack of corrugated single layers of VO_5 units having a step of ~2.9 Å, with the layers being closely related to those occurring in crystalline V_2O_5.[1] On the other hand, Oka et al.[7] proposed that $V_2O_5 \cdot nH_2O$ is made of V_2O_5 bilayers according to the crystalline structure of $A_xV_2O_5$ (A = Na, K).[8] This model is further supported by recent polarized X-ray absorption and XAFS studies on deposited films of $V_2O_5 \cdot nH_2O$.[9] Both Livage and Oka models account for the interatomic vector of ~2.9 Å appearing in the 1-D Patterson maps constructed from X-ray diffraction (XRD)

* To whom correspondence should be addressed. E-mail: kanatzid@cem.msu.edu.
[†] Department of Physics and Astronomy and Center for Fundamental Materials Research, Michigan State University.
[‡] Brookhaven National Laboratory.
[§] Department of Chemistry and Center for Fundamental Materials Research, Michigan State University.

(1) (a) Livage, J.; Pelletier, O.; Davidson, P. *J. Sol.-Gel Sci. Technol*. **2000**, *19*, 275. (b) Livage, J. *Chem. Mater*. **1991**, *3*, 578.
(2) (a) Raju, A. R.; Rao, C. N. R. *J. Chem. Soc., Chem. Commun.* **1991**, *18*, 1260. (b) Imawan, C.; Steffes, H.; Solzbacher, F.; Obermeier, F. *Sens. Actuators* **2001**, *B77*, 346.
(3) Sanchez, C.; Morineau, R.; Livage, J. *Phys. Status Solidi* A **1983**, *76*, 661.
(4) (a) Shoji, E.; Butty, D. A. *Electrochim. Acta* **2000**, *45*, 3757. (b) Goward, G. G.; Leroux, F.; Nazar, L. F. *Electrochim. Acta* **1998**, *43*, 1307. (c) Lira-Cantu, M.; Gomez-Romero, P. *J. Electrochem. Soc.* **1999**, *146*, 4139.
(5) (a) Kanatzidis, M. G.; Wu, C. G.; Marcy, H. O.; Kannewurf, C. R. *J. Am. Chem. Soc*. **1989**, *111*, 4139. (b) Kanatzidis, M. G.; Wu, C. G.; Marcy, H. O.; DeGroot, D. C.; Kannewurf, C. R. *Chem. Mater*. **1990**, *2*, 222. (c) Wu, C. G.; DeGroot, D. C.; Marcy, H. O.; Schindler, J.; Kannewurf, C. R.; Liu, Y. J.; Hirpo, W.; Kanatzidis, M. G. *Chem. Mater*. **1996**, *8*, 1992.
(6) Petkov, V.; Billinge, S. J. L.; Larson, P.; Mahanti, S. D.; Vogt, T.; Rangan, K. K.; Kanatzidis, M. G. *Phys. Rev. B* **2002**, *65*, 092105.
(7) (a) Yao, T.; Oka, Y.; Yamamoto, N. *J. Mater. Chem.* **1992**, *2*, 337. (b) Yao, T.; Oka, Y.; Yamamoto, N. *Mater. Res. Bull.* **1992**, *27*, 669. (c) Yao, T.; Oka, Y.; Yamamoto, N. *J. Mater. Chem.* **1992**, *2*, 331.
(8) (a) Kanke, Y.; Kato, K.; Takayama-Muromachi, E.; Isobe, M. *Acta Crystallogr.* **1990**, *C46*, 536. (b) Kanke, Y.; Kato, K.; Takayama-Muromachi, E.; Isobe, M.; Kosuda, K.; *Acta Crystallogr.* **1992**, *C46*, 1590.
(9) Giorgetti, M.; Passerini, S.; Smyl, W. H. *Inorg. Chem.* **2000**, *39*, 1514.

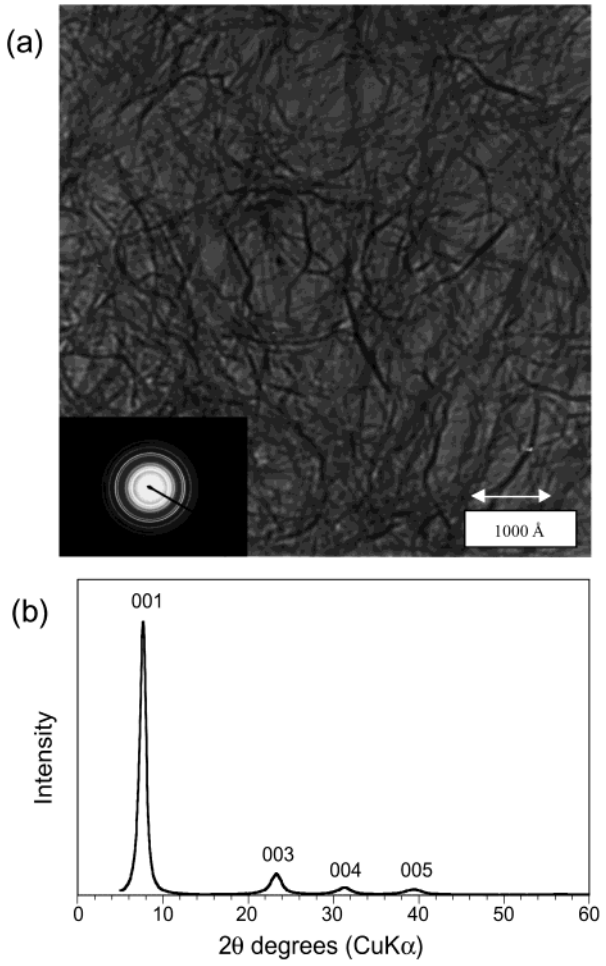

Figure 1. Representative transmission electron microscopy (TEM) image (a), and powder XRD pattern in reflection geometry (b) of the $V_2O_5 \cdot nH_2O$ xerogel.

patterns of $V_2O_5 \cdot nH_2O$. However, neither model can fully explain the observed XRD patterns nor provide a description of the atomic structure in terms of meaningful parameters such as a unit cell and atomic coordinates.

In this paper, we describe the determination of the 3-D structure of $V_2O_5 \cdot nH_2O$ by the atomic pair distribution function (PDF) technique. This technique has emerged recently as a powerful and unique tool for structural characterization of crystalline materials with significant intrinsic disorder.[6,10] The strength of the technique stems from the fact that it takes both the Bragg as well as the diffuse component of the diffraction data into account and thus yields structure parameters reflecting both the long-range order and the local structural disorder in materials. In contrast, other techniques employed to study polycrystalline materials (e.g., Rietveld[11]) use Bragg peaks alone and are not very sensitive to disorder. Here, we show that the structure of $V_2O_5 \cdot nH_2O$ xerogel can be well described as an assembly of well-defined bilayers of single V_2O_5 layers made of square pyramidal VO_5 units with water molecules residing between them. The new and direct structure information reported here explains well the observed properties of $V_2O_5 \cdot nH_2O$ xerogel and broadens our understanding of this material.

(10) (a) Petkov, V.; Billinge, S. J. L.; Heising, J.; Kanatzidis, M. G. *J. Am. Chem. Soc.* **2000**, *122*, 11571. (b) Petkov, V.; Billinge, S. J. L. *Physica B* **2001**, *305*, 83.

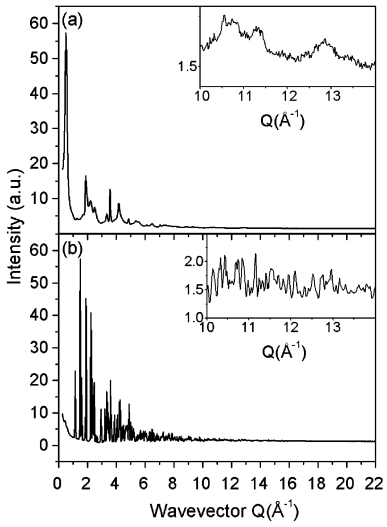

Figure 2. X-ray diffraction patterns of (a) $V_2O_5 \cdot nH_2O$ xerogel and (b) crystalline V_2O_5 obtained in transmission geometry. The high-Q portion of the data which contains key structural information is given in an expanded scale in the inset.

Experimental Section

Sample Preparation. Crystalline V_2O_5 was purchased from Aldrich. The $V_2O_5 \cdot nH_2O$ xerogel was synthesized by melting of crystalline V_2O_5 at ~800 °C and pouring the melt into deionized water under vigorous stirring. The resulting dark red solution transformed to gel within 4 days. The gel was cast on a glass plate and allowed to dry at room temperature until a dark red-brown film was formed. The film was peeled off the glass plate and ground into fine powder for the diffraction experiments. The water content, n, was determined by thermogravimetric analysis (TGA) to be approximately between 1.6 and 2.0. This is consistent with the observed interlayer spacing of 11.5 Å. This spacing in $V_2O_5 \cdot nH_2O$ xerogel is very sensitive to the amount of water encapsulated between the V_2O_5 layers.[7]

X-ray Diffraction Experiments. Two samples were investigated, crystalline V_2O_5 and $V_2O_5 \cdot nH_2O$ xerogel. The samples were carefully packed between Kapton foils to avoid texture formation and subjected to diffraction experiments with X-rays of energy 29.09 keV ($\lambda = 0.4257$ Å). The higher energy X-rays were used to extend the region of reciprocal space covered (i.e., to obtain data at higher wave vectors, Q), which is important for the success of PDF analysis. The measurements were carried out in symmetric transmission geometry at the beam line X7A of the National Synchrotron Light Source (NSLS), Brookhaven National Laboratory. Scattered radiation was collected with an intrinsic germanium detector connected to a multichannel analyzer. Several runs were conducted, and the resulting XRD patterns were averaged to improve the statistical accuracy and reduce any systematic effect due to instabilities in the experimental setup. The diffraction patterns obtained are shown in Figure 2. As can be seen, the XRD pattern of crystalline V_2O_5 (Figure 2b) exhibits well-defined Bragg peaks up to a very high wave vector $Q \approx 13-15$ Å^{-1} ($Q = 4\pi \sin\theta/\lambda$). The material is obviously a well-crystallized solid with no positional disorder at the atomic scale. The XRD pattern of $V_2O_5 \cdot nH_2O$ xerogel (Figure 2a), on the other hand, contains a few Bragg-like features and a pronounced diffuse component. This is particularly evident in the inset of Figure 2a which shows the high Q data on an expanded scale. Such a pattern, which is usually observed in materials with significant disorder, is practically impossible to account for by ordinary techniques for structure determination, such as the Rietveld technique. However, as we will demonstrate, once reduced to the corresponding atomic PDF, it becomes a structure-sensitive quantity lending itself to structure determination.

(11) Rietveld, H. M. *J. Appl. Crystallogr.* **1969**, *2*, 65.

PDF Analysis of the Diffraction Data. The frequently used atomic PDF, also called $G(r)$, is defined as follows:

$$G(r) = 4\pi r[\rho(r) - \rho_o] \quad (1)$$

where $\rho(r)$ and ρ_o are the local and average atomic number densities, respectively, and r is the radial distance. $G(r)$ gives the number of atoms in a spherical shell of unit thickness at a distance r from a reference atom. It peaks at characteristic distances separating pairs of atoms and thus reflects the atomic structure. $G(r)$ is the Fourier transform of the experimentally observable total structure function,[12] $S(Q)$, that is

$$G(r) = (2/\pi) \int_{Q=0}^{Q_{max}} Q[S(Q) - 1] \sin(Qr) dQ \quad (2)$$

where Q is the magnitude of the wave vector. The structure function is related to the coherent part of the total diffracted intensity of the material as follows:

$$S(Q) = 1 + [I^{coh}(Q) - \sum c_i |f_i(Q)|^2] / |\sum c_i f_i(Q)|^2 \quad (3)$$

where $I^{coh}(Q)$ is the coherent scattering intensity per atom in electron units, and c_i and f_i are the atomic concentration and X-ray scattering factor, respectively, for the atomic species of type i.[12] As can be seen from eqs 1−3, $G(r)$ is simply another representation of the diffraction data. However, exploring the diffraction data in real space is advantageous, especially in the case of materials with significant structural disorder. First, as eq 3 implies, the *total* scattering, including Bragg scattering as well as diffuse scattering, contributes to the PDF. In this way, both the long-range atomic structure, manifested in the sharp Bragg peaks, and the local nonperiodic structural imperfections, manifested in the diffuse components of the diffraction pattern, are reflected in the PDF. Second, by accessing high values of Q, experimental $G(r)$'s with high real-space resolution can be obtained and, hence, quite fine structural features revealed.[13] In fact, data at high Q values ($Q > 15$) are critical to the success of PDF analysis. Third, $G(r)$ is barely influenced by diffraction optics and experimental factors because these are accounted for in the step of extracting the coherent intensities from the raw diffraction data. This renders the PDF a *structure-dependent quantity* that gives directly relative positions of atoms in materials. As demonstrated here, this enables convenient testing and refinement of structural models.

Experimental PDFs for crystalline V_2O_5 and $V_2O_5 \cdot nH_2O$ xerogel were obtained as follows. First, the coherently scattered intensities were extracted from the XRD patterns of Figure 2 by applying appropriate corrections for flux, background, Compton scattering, and sample absorption. The intensities were normalized in absolute electron units and reduced to structure functions $S(Q)$ defined in eq 3. Finally, the $S(Q)$ data were weighted by the corresponding wave vectors, Q, and Fourier transformed according to eq 2 to obtain the atomic PDFs. All data processing was done using the program RAD.[14] The resulting experimental structure functions are shown in Figure 3 and the corresponding PDFs, $G(r)$, in Figure 4. A comparison between the data in Figures 2 and 3 exemplifies the different way the same diffraction features show up in the powder XRD patterns and the structure functions extracted from them. As can be seen in Figure 2, the XRD patterns are dominated by strong Bragg peaks at low wave vectors and hardly show the weak but critically important diffraction features at higher wave vectors Q. In other words, XRD patterns are an experimental quantity mainly sensitive to long-range atomic ordering in materials. In contrast, reduced structure functions (i.e., $Q[S(Q) - 1]$) extracted from the XRD patterns according to eq 3 cause all diffraction features including those at higher values of Q to appear strong; see Figure 3. This enhances the sensitivity to local atomic ordering and makes the Fourier couple $Q[S(Q) - 1]/G(r)$ (i.e., PDF), see eq 2, an experimental quantity well suited to study materials of limited structural coherence. The fact that $V_2O_5 \cdot nH_2O$ xerogel has limited structural coherence is clearly seen in the inset in Figure 4a showing the corresponding PDF decaying to zero already at $r \approx 50$ Å. In contrast, the PDF of a crystal, such as V_2O_5, persists to much higher real space distances (see the inset in Figure 4b).

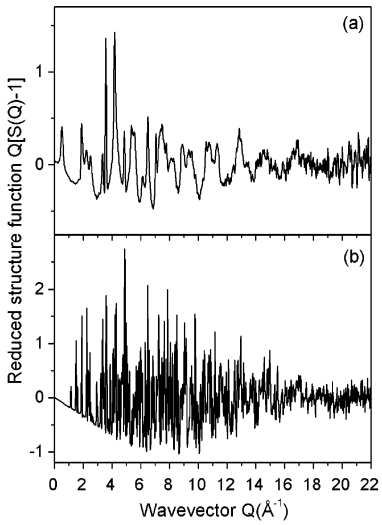

Figure 3. Reduced structure functions, $Q[S(Q) - 1]$, of (a) $V_2O_5 \cdot nH_2O$ xerogel and (b) crystalline V_2O_5 derived from the XRD patterns of Figure 2.

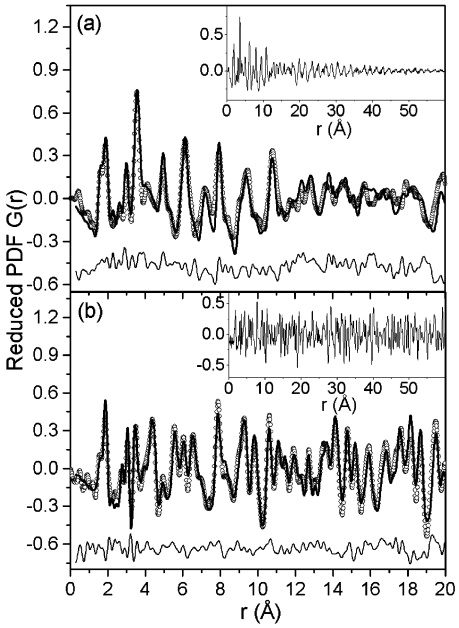

Figure 4. Experimental (○) and fitted (−) PDFs for (a) $V_2O_5 \cdot nH_2O$ xerogel and (b) crystalline V_2O_5. The residual difference is shown in the lower part. The experimental data are shown in an expanded scale and over very large interatomic distances r in the inset.

Results

Even though the structure of crystalline V_2O_5 is well known, it was used here as a standard to illustrate the capabilities of the PDF technique. A structural model based on the 14-atom

(12) (a) Klug, H. P.; Alexander, L. E. *X-ray Diffraction Procedures for Polycrystalline Materials*; Wiley: New York, 1974. (b) Waseda, Y. *The Structure of Noncrystalline Materials*; McGraw-Hill: New York, 1980.
(13) (a) Petkov, V.; Jeong, I.-K.; Chung, J. S.; Thorpe, M. F.; Kycia, S.; Billinge, S. J. L. *Phys. Rev. Lett.* **1999**, *83*, 4089. (b) Petkov, V.; Billinge, S. J. L.; Shastri, S. D.; Himmel, B. *Phys. Rev. Lett.* **2000**, *85*, 3436.
(14) Petkov, V. *J. Appl. Crystallogr*. **1989**, *22*, 387.

Table 1. Positional Parameters (*x*,*z*) of V and O in Orthorhombic V_2O_5 As Determined by Traditional Diffraction Experiments[15] and the Present PDF Work[a]

atom	*x*([15])	*x*(PDF)	*z*([15])	*z*(PDF)
V	0.148	0.1484(2)	0.105	0.1083(2)
O(1)	0.149	0.1481(4)	0.458	0.4604(4)
O(2)	0.320	0.3145(4)	0.000	−0.0090(4)
O(3)	0	0	0.000	0.0170(4)

[a] V, O1, and O2 occupy the Wyckoff position (4f), and O3 occupies the position (2a) in space group *Pmmn* (origin choice one).

unit cell of V_2O_5[15] was fit to the experimental PDF and structure parameters such as unit cell constants, atomic coordinates, and thermal factors refined so as to obtain the best possible agreement between the calculated and experimental data. The fit was done with the program PDFFIT[16] and was constrained to have the symmetry of the *Pmmn* space group. In comparing with experiment, the model PDF was convoluted with a Sinc function, $S(r) = \sin(Q_{max}r)/r$, to account for the finite Q_{max} of the data.[16] The usual goodness-of-fit indicator, R_G

$$R_G = \left\{ \frac{\sum w_i (G_i^{exp} - G_i^{calc})^2}{\sum w_i (G_i^{exp})^2} \right\}^{1/2} \quad (4)$$

was used to estimate the success of structure refinement. Here G^{exp} and G^{calc} are the experimental and calculated PDFs, respectively, and the w_i's are weighting factors reflecting the statistical quality of the individual data points. The quality of the present PDFs was estimated, and the individual w_i's were determined with the help of the program IFO.[17] The program employs statistical procedures based on the maximum entropy method to estimate the experimental uncertainty in each PDF data point; the reciprocal of this uncertainty was used as w_i. The best fit achieved is shown in Figure 4b, and the corresponding value of R_G is 24%.[18] The PDF-based fit yielded the following cell constants for V_2O_5: $a = 11.498(3)$ Å, $b = 3.545(3)$ Å, $c = 4.345(3)$ Å. They are in good agreement with those obtained by traditional diffraction experiments: $a = 11.519$ Å, $b = 3.564$ Å, $c = 4.373$ Å.[15] The refined atomic positions are also in good agreement with previous results; see Table 1. This agreement well documents the fact that the atomic PDF provides a reliable quantitative basis for structure determination.

The structure of $V_2O_5 \cdot nH_2O$ xerogel was determined as follows. At first, Livage's model featuring the xerogel as a stack of corrugated single layers of VO_5 was attempted. The model was based on a 228-atom cell constructed according to the scheme suggested by Livage et al.[1] with the help of the software package Cerius[2];[19] see Figure 5. As can be seen in Figure 6a, this model does not reproduce the experimental data especially in the region of *r* values from 2 to 12 Å. Furthermore, the model is inconsistent with the material's measured density[20] and thus is ruled out as a possible structure of $V_2O_5 \cdot nH_2O$.

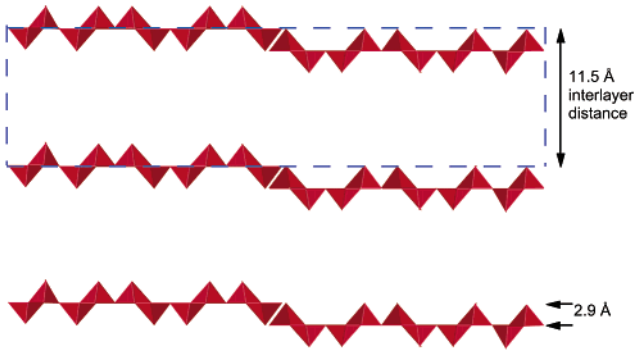

Figure 5. Corrugated structural model for the $V_2O_5 \cdot nH_2O$ xerogel, proposed by Livage et al.[1] The model was constructed using the software package Cerius[2].

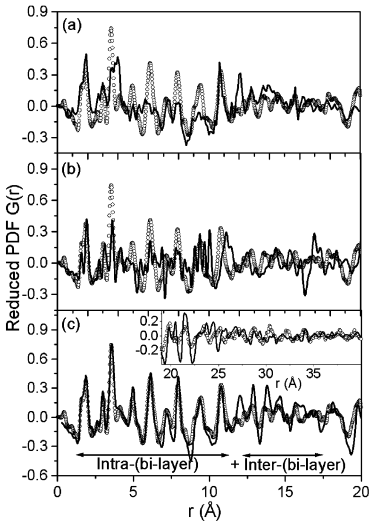

Figure 6. Comparison between the experimental PDF for $V_2O_5 \cdot nH_2O$ (○) and model PDFs (−) for (a) assembly of corrugated single layers of VO_5 polyhedra as suggested by Livage,[1] (b) distorted V_3O_8-type structure,[17] and (c) assembly of perfectly stacked bilayers of VO_5 polyhedra (correct structure).

A model featuring layers of (V−O) polyhedra stacked according to the structure of $H_2V_3O_8$[21] (not shown) was attempted as well. This model did not agree with the experimental data either, as can be seen in Figure 6b. This prompted us to explore models involving bilayers of V−O polyhedra as suggested by Oka et al. As a starting model structure, we considered that found in $Na_{0.5}V_2O_5$.[8] This structure features V_2O_5 bilayers stacked along the *c*-axis of a monoclinic unit cell (space group *C*2/*m*) with parameters: $a = 11.663$ Å, $b = 3.653$ Å, $c = 8.92$ Å, and $\beta = 90.91°$. To account for the fact that the xerogel interlayer distance is 11.5 Å, we expanded the structure of the $Na_{0.5}V_2O_5$ model along the *c*-direction and adjusted the *z*-coordinates of all 32 atoms in the starting unit cell accordingly. In addition, we placed oxygen atoms representing water

(15) Wyckoff, R. *Crystal Structures*; Wiley: New York, 1964.
(16) Proffen, T.; Billinge, S. J. L. *J. Appl. Crystallogr.* **1999**, *32*, 572.
(17) Petkov, V.; Danev, R. *J. Appl. Crystallogr.* **1998**, *31*, 609.
(18) The agreement factor is 13% when the atomic distribution functions $g(r) = \rho(r)/\rho_0$ and not $G(r)$'s are compared to each other. Both agreement factors appear high when compared to the agreement factor, R_{WP}, of 8% obtained for crystalline V_2O_5 data refined by the Rietveld method. This does not indicate an inferior structure refinement, but merely reflects the fact that the atomic pair distribution function being fit differs from the XRD pattern typically fit in a Rietveld refinement. The R_{WP} value from Rietveld is a function minimized in *reciprocal* space whereas R_G is minimized in *real* space and as such is a much more sensitive quantity to local ordering in materials. As a result, R_W's greater than 15% are common with PDF refinements of well-crystallized materials.[6,10] The inherently higher absolute value of the goodness-of-fit factors resulting from PDF-based refinements does not affect its functional purpose as a residual function that must be minimized to find the best fit and as a quantity allowing one to differentiate between competing structural models.
(19) *Cerius*[2] *Modeling Environment*; Molecular Simulations Inc.: San Diego, April 1999.
(20) Liu, Y.-J.; Cowen, J. A.; Kaplan, T. A.; DeGroot, D. C.; Schindler, J.; Kannewurf, C. R.; Kanatzidis, M. G. *Chem. Mater.* **1995**, *7*, 1616.
(21) Oka, Y.; Yao, T.; Yamamoto, N. *J. Solid State Chem.* **1990**, *89*, 372.

Table 2. Positional Parameters (x,z) and Isotropic Thermal Factors, U_{iso}, of V and O in Monoclinic $V_2O_5 \cdot nH_2O$ with Lattice Parameters $a = 11.722(3)$ Å, $b = 3.570(3)$ Å, $c = 11.520(3)$ Å, and $\beta = 88.65°$ Obtained by a PDF-Based Refinement[a]

atom	x	z	U_{iso} [Å^2]
V(1)	0.9317(2)	0.1303(2)	0.007(1)
V(2)	0.2227(2)	0.1332(2)	0.007(1)
O(1)	0.3955(4)	0.1035(4)	0.033(1)
O(2)	0.07521(4)	0.0950(4)	0.033(1)
O(3)	0.7537(4)	0.0658(4)	0.033(1)
O(4)	0.9046(4)	0.2670(4)	0.033(1)
O(5)	0.2018(4)	0.2669(4)	0.033(1)
O*	0.6065(4)	0.5085(4)	0.030(1)

[a] V and O occupy the Wyckoff position (4i) in space group $C2/m$. O* stands for oxygen atoms from water molecules.

molecules on the Na sites to generate a sheet of water molecules between the V−O layers which is close to the experimentally determined water content. Hydrogen atoms were not considered because of their negligible contribution to the experimental diffraction data. This model was refined against the experimental data observing the constraints of space group $C2/m$ and converged rapidly. The very good agreement between the calculated and measured PDFs is shown in Figure 6c. The value of the corresponding goodness-of-fit indicator R_G was 34%. It is 19% when $g(r)$'s and not $G(r)$'s are compared to each other. The refined lattice parameters, atomic positions, and isotropic thermal factors are summarized in Table 2.

Discussion

An important outcome of the present PDF study is that it yields the atomic structure of $V_2O_5 \cdot nH_2O$ xerogel in terms of a relatively simple model with only few meaningful parameters such as a unit cell and symmetry. In other words, this material is much more ordered than was previously thought. The present study unambiguously shows that the xerogel indeed possesses a significant degree of atomic ordering (enough perhaps to be characterized as nanocrystalline), something that is difficult to appreciate by considering the XRD pattern alone. The small number of parameters needed to describe the 3-D atomic structure will facilitate future electronic band-structure calculations, making it easier to understand and predict structure-dependent properties of this technologically promising material.

An inspection of the refined structure parameters of Table 2 and the data in Figure 6 reveals the following characteristic features of the atomic structure in $V_2O_5 \cdot nH_2O$. In contrast to crystalline V_2O_5, which is an ordered assembly of single layers of V_2O_5, the xerogel is a stack of long ribbonlike slabs which are bilayers of single V_2O_5 layers made up of square pyramidal VO_5 units; see Figures 7 and 8a. The distance of closest approach between the bilayers is approximately 11.5 Å, and this is the most noticeable period of repetition in the structure as manifested by the strength and position of the lowest-Q peak in the XRD pattern (see Figures 1b and 2a). It is this distance that expands (or contracts) as the xerogel absorbs guest molecules in its structure. The distance between the two single sheets of V_2O_5, making up the bilayer, is close to 2.90 Å (indicated in Figure 7.) The proposed model viewing the xerogel as an assembly of stacked bilayers well explains the presence of an interatomic distance of 2.9 Å in the 1-D Paterson maps constructed from X-ray powder patterns of the material. In our model, this is the distance between the two sheets of V_2O_5 layers

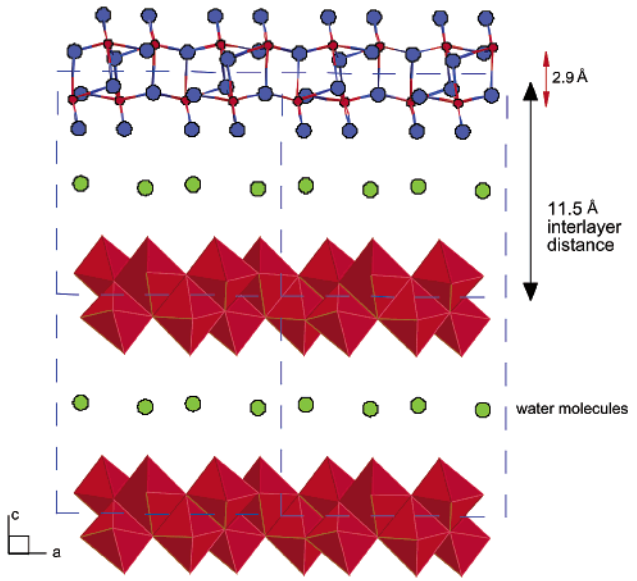

Figure 7. Structure of $V_2O_5 \cdot nH_2O$ xerogel (polyhedra and ball-stick model) as revealed by PDF analysis. Characteristic distances are shown. Water molecules are shown in green.

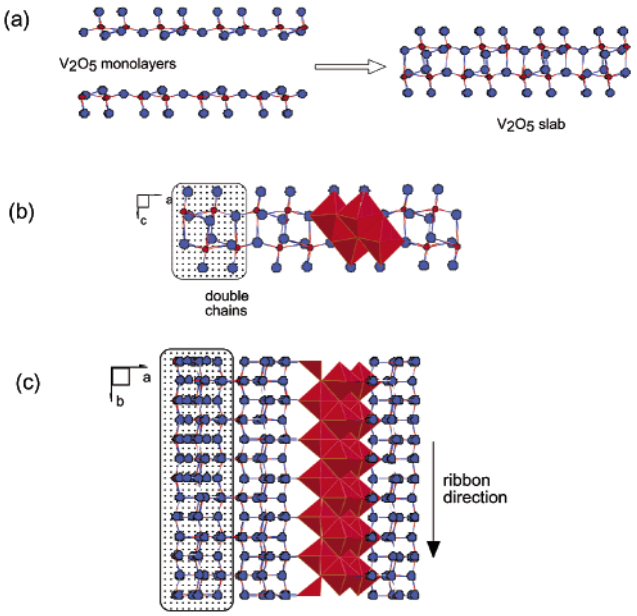

Figure 8. (a) Approach of two single V_2O_5 layers to give a bilayer V_2O_5 slab. Each V_2O_5 single layer is made of square pyramidal VO_5 units. (b) The highlighted block and polyhedral sections feature the location of double chains within the V_2O_5 slabs. View is down the chain direction. (c) Rotation of object shown in (b) by 90°, showing disposition of parallel double chains.

making up a bilayer slab. Because, as our study shows, the slabs are quite ordered, there is no surprise that the Patterson maps (when projected on the c-axis) show a peak at this characteristic intralayer distance.

The oxygen coordination of V atoms in $V_2O_5 \cdot nH_2O$ is similar to that in crystalline V_2O_5 resembling a square pyramid, with four oxygens at distances from 1.79 to 2.10 Å making the base of the pyramid and an oxygen atom at ∼1.6 Å capping the pyramid. The latter amounts to a V═O double bond, the existence of which is well known from infrared spectroscopy. These distinct V−O bonds are the main contributor to the first, almost resolved peak-splitting in the experimental PDF; see

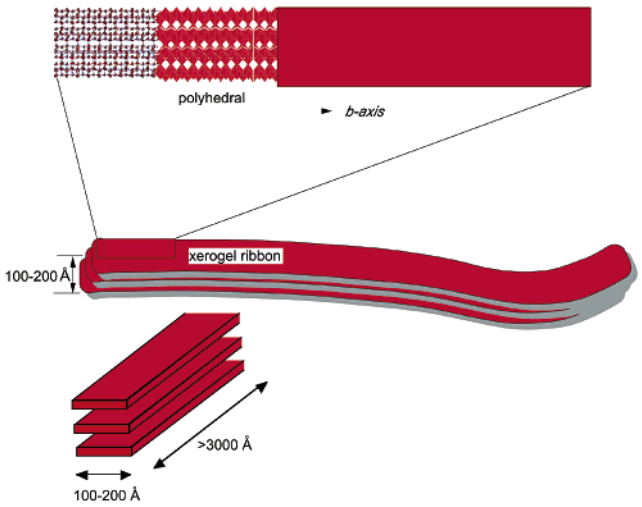

Figure 9. Ribbonlike representation of $V_2O_5 \cdot nH_2O$ xerogel showing intermediate structural makeup and overall V_2O_5 slab organization.

Figure 4. A sixth oxygen atom occupies what would be the six coordination site (opposite to the doubly bonded V═O oxygen) at a much longer distance of ~2.5 Å.

If the coordination environment of V atoms in each bilayered slab is taken as octahedral (local distortion notwithstanding), then the structure of each V_2O_5 slab can be understood as follows. The VO_6 octahedra share edges to from double chains propagating down the *b*-axis as shown in Figure 8. These double chains then arrange in parallel and side by side via interchain V−O bonds (by sharing corners of octahedra) to form the slab; see Figure 8b,c. In this connectivity motif, intrachain V−O bonding is more extensive than interchain bonding. A similar situation exists in crystalline V_2O_5, which also has slabs (albeit monolayered) composed of parallel double chains. This chain-based slab structure in both crystalline V_2O_5 and $V_2O_5 \cdot nH_2O$ xerogel creates a one-dimensional "bias" to the structure that is responsible for the needlelike crystal growth in the former and the formation of long nanoribbons in the xerogel; see model in Figure 9.

A more careful inspection of the experimental and model PDFs for $V_2O_5 \cdot nH_2O$ xerogel in Figure 6c shows, however, an excellent match up to distances as long as 11.5 Å, which is exactly the distance of closest approach between two bilayers in $V_2O_5 \cdot nH_2O$. The model PDF appears somewhat sharper than the experimental one at higher *r*-values ranging from 11.5 Å to ~15 Å. At $r > 15$ Å, the model and experimental data line up again. A similar sharpening of the model data with respect to the experiment is observed over distances 21−25 Å as well; see the inset in Figure 6c. This range of *r* values corresponds to the separation between two next-nearest slabs in $V_2O_5 \cdot nH_2O$ (i.e., 2×11.5 Å). Such a slight but persistent loss of structural coherence repeatedly occurring at distances close to the interslab separation suggests that the slabs in $V_2O_5 \cdot nH_2O$ are not stacked in perfect registry; that is, they are somewhat turbostratically disordered. To check this hypothesis, we refined our model further to mimic poorly stacked slabs of the type shown in Figure 9. The modification was done by artificially enlarging the atomic thermal factors in the out-of-plane (*z*) direction, that is, the plane of slabs, thus effectively reducing the slab−slab correlations. Such an approach has proved quite successful in modeling disorder in materials with significant turbostratic disorder such as pyrolytic graphite.[22] The modified model yielded the PDF shown in Figure 4a and lowered the goodness-of-fit indicator *R* to 28% (15% in the case of $g(r)$'s). The better agreement achieved supports the general and well-accepted view that the slabs in $V_2O_5 \cdot nH_2O$ xerogel are not stacked in registry. This is in contrast to the considerable layer−layer correlation occurring in "restacked" WS_2.[10a]

Conclusions

The full 3-D structure of $V_2O_5 \cdot nH_2O$ xerogel has been determined for the first time using the atomic PDF technique. The structure differs from that of crystalline V_2O_5 and is consistent with the one proposed by Oka et al. At the atomic scale, the xerogel can be well described as a double layer of V_2O_5 stacked along the *c*-axis of a monoclinic unit cell. The stacking sequence is imperfect, confirming the widespread view of the extensive turbostratic disorder in this system. This structure explains all known spectroscopic, physical, and chemical observations associated with this material. Settling the structural issue in this interesting material should open new approaches in experimentation and new insights into how to better exploit its properties in the future. The present study also provides an excellent example of the great potential of the PDF technique in determining structures of poorly diffracting and nanocrystalline materials. What still remains to be answered is (a) what is the chemical structure at the ribbon edges (i.e., how are the ribbons terminated?) and (b) are there any cationic species intercalated between the ribbon slabs? For example, the presence of $(H_3O)^+$ cations or small amounts of $[VO(H_2O)_5]^{2+}$ cannot be detected by a PDF study of the type described here.

Acknowledgment. This work was supported by NSF Grant CHE 99-03706 and DMR-0127644. NSLS is supported by the U.S. Department of Energy through DE-AC02-98-CH10886.

JA026143Y

(22) Petkov, V.; DiFrancesco, R. G.; Billinge, S. J. L.; Acharaya, M.; Foley, H. C. *Philos. Mag. B* **1999**, *79*, 1519.